Top Catal (2013) 56:1074–1081
DOI 10.1007/s11244-013-0072-8

ORIGINAL PAPER

# Spectroscopic Evidences of Charge Transfer Phenomena and Stabilization of Unusual Phases at Iron Oxide Monolayers Grown on Pt(111)

**Livia Giordano · Gianfranco Pacchioni · Claudine Noguera · Jacek Goniakowski**

Published online: 18 June 2013


**Abstract** Strong electrostatic coupling between the local structure of metal-supported oxide ultra-thin films and the charge state of adsorbed species (such as Au atoms and $O_2$ molecules) is at the origin of a co-existence of alternative adsorption configurations, with drastically different structural and electronic characteristics. This effect may contribute also to the stabilization of oxide phases of unusual stoichiometries, where the ion valences are compensated by an electron exchange with the metal substrate. We report an analysis of the spectroscopic signatures of such differently charged adsorbates and unusual oxide phases, including valence and core electrons spectroscopies and vibrational characteristics. We show that the adsorbate charge states can be identified by their signature in the electronic states around the Fermi level and by the modification of the vibrational frequencies of adsorbed probe molecules. Moreover, core level analysis may contribute to the identification of the oxygen-rich phase, formed at high oxygen exposure. The detailed theoretical investigation of the spectroscopic signatures of alternative adsorption configurations and adsorbate charge states supplies a set of data, which may help the experimental identification of such species.

**Keywords** Spectroscopy of iron oxide monolayers · Oxides · Ultra-thin films · Spectroscopies · DFT calculations

L. Giordano (✉) · G. Pacchioni
Dipartimento di Scienza dei Materiali, Università di Milano-Bicocca, via Cozzi, 53, 20125 Milan, Italy
e-mail: livia.giordano@mater.unimib.it

C. Noguera · J. Goniakowski
INSP, UMR 7588, CNRS and UPMC Université Paris 06, 4 Place Jussieu, 75252 Paris Cedex 05, France

## 1 Introduction

Oxide-supported metal nano-particles are relevant in heterogeneous catalysis since they display an enhanced reactivity with respect to bulk materials [1–6]. The most noticeable example is represented by gold, well known to be an inert metal, which manifests catalytic activity when in nano-metric clusters grown on oxide surfaces [7, 8].

In the case of reducible oxide supports, like ceria, titania, magnetite, etc., the metal nano-particles may undergo the so called strong metal support interaction (SMSI). Under reaction conditions (namely high temperature and high gas pressure) a mass transport may occur from the support to the nano-particle, which can even be encapsulated by a thin oxide layer [9]. The role of this oxide thin film on the reactivity of the metal nanoparticle depends on the system. While, in many cases, it inhibits reactions taking place on the metal facets, in some cases, it has been shown to enhance the reactivity of the supported nanoparticles [10].

Indeed, oxide ultra-thin films on metal surfaces, or on metal nanoparticles subject to SMSI, may display unusual properties, completely different from the surfaces of bulk oxides. For instance, because of the nano-dimensionality, the film can adopt unconventional structures, giving rise to complex phase diagrams [11, 12]. Furthermore, when the thickness is of a few atomic layers only, the metallic substrate may influence the properties of the film, acting, for instance, as a source or a sink of electrons [13]. For these reasons, by varying the nature of the oxide and/or of the metal, the thickness of the oxide film, and the interfacial structure (network of dislocations, Moiré patterns, etc.) the properties of these films can be finely tuned.

The iron oxide/platinum combination represents an especially suitable system for an investigation of the

reactivity of nano-particles subjected to SMSI. Indeed, encapsulation of Pt nanoparticles grown on $Fe_3O_4(111)$ takes place after annealing in ultra-high vacuum (UHV) conditions above 800 K. Interestingly, the oxide layer which is formed on the exposed Pt(111) facet has FeO stoichiometry and has exactly the same structure as the FeO monolayer which can be epitaxially grown on the Pt(111) single-crystal surface [14]. Furthermore, both the FeO/Pt(111) film and the encapsulated Pt nano-particles on $Fe_3O_4(111)$ show an enhanced reactivity towards CO oxidation [15–17]. The reaction mechanism involves the incorporation of oxygen in the film exposed to high oxygen pressures (in the mbar range) [15]. The so formed oxygen-rich film of $FeO_{2-x}$ stoichiometry, is shown to easily oxidize CO [16]. The reactivity of the FeO/Pt(111) film is also maintained when the film is exposed to air or to a mixture of $O_2$ and $H_2O$ [18], with relevant implications for possible use in catalysis. This example shows that the oxide layers grown on metal single crystal surfaces may represent a model for metal nano-particles subjected to SMSI, and enable the use of all the spectroscopic techniques available in surface science as well as of theoretical modeling.

The FeO/Pt(111) film has been extensively characterized [19]. It consists of a FeO mono-layer and presents a Moiré superstructure, due to the lattice mismatch between the FeO and Pt, with a periodicity of about 25 Å [20]. While the FeO(111) mono-layer is flat when unsupported, on Pt it presents a considerable rumpling due to an electron transfer from the oxide to the metal. The interlayer distance between the interfacial Fe and the surface O layers has been estimated to be in average 0.68 Å (half of the bulk one in the (111) direction) [21]. Because of the ionic nature of the oxide, this support-induced film distortion creates a dipole moment which opposes and partly compensates the dipole moment due to the interfacial charge transfer [22]. These electrostatic effects and the compression of the substrate charge density by the oxide film make the work function of an oxide/metal system considerably different from that of the bare metal [23, 24]. In the case of FeO/Pt(111) the different contributions nearly cancel each other and the average work function of the combined system is almost the same as for bare Pt(111). However, the variation of the structural characteristics along the Moiré pattern changes the weight of the different contributions, producing a modulation of the surface potential [25–27]. Recent STM measurements and DFT calculations by using the complete Moiré unit cell have shown that the surface potential follows the sequence Fe-top (O-fcc) < Fe-hcp (O-top) < Fe-fcc (O-hcp) [27, 28]. The modulation of the surface potential affects the adsorption properties by creating preferential adsorption sites and resulting in a ordered array of adsorbates, as reported for the case of Au adatoms [29].

In this paper we reconsider some peculiar adsorption properties of FeO/Pt(111) films, involving charge transfers to/from adsorbed Au and $O_2$ and a strong coupling between local atomic structure and adsorbate charge state. We compute the corresponding spectroscopic characteristics which may help the experimental identification of the adsorption mode. Moreover, a detailed analysis of the spectroscopic characteristics of films of different compositions, which appear in the phase diagram as a function of the oxygen and water chemical potentials, is carried out and compared with the available experimental data.

## 2 Computational Method

The structural, electronic and magnetic properties of FeO monolayers deposited on Pt(111) have been theoretically addressed in several papers, with reduced pseudomorphic, non-pseudomorphic [26, 30], and complete Moiré unit cell model [27].

The results of this paper are obtained with pseudomorphic interface models and (2 × 2) unit cells already used in our previous studies [18, 31], which show a good agreement with the few existing estimations obtained in calculations with the full Moiré cell [27, 28]. In the pseudomorphic model each high-symmetry region present in the Moiré is described separately by a specific unit cell, where the lattices are aligned and the Pt(111) substrate is expanded in order to match the oxide in-plane lattice parameter. We use a plane waves DFT + U approach [32] ($U_{Fe}-J_{Fe} = 3$ eV, correctly describing FeO and $Fe_2O_3$ bulk oxides), PW91 functional [33] and projector augmented wave (PAW) pseudopotentials [34, 35], as implemented in VASP [36, 37]. The Pt surface is represented by a five atomic layer slab, with oxide and ad-species adsorbed on one side, and dipole correction applied in order to eliminate the spurious interaction between repeated replica. All adsorbate and oxide coordinates are fully relaxed, while Pt is relaxed only in z direction (threshold on forces = 0.01 eV/Å), in order to avoid spurious relaxations induced by the imposed strain. Since the antiferromagnetic coupling is preferred in the oxide film [26], a row-wise RW-(2 × 1) antiferromagnetic ordering of the Fe ions is imposed, with alternating dense rows of cations with opposite magnetization. Atomic charges are estimated by Bader decomposition method [38].

Adsorbate binding energies have been computed as: $E_{ads} = E_{film} + E_{adsorbate} - E_{adsorbate/film}$, where $E_{film}$, $E_{adsorbate}$ and $E_{adsorbate/film}$ are the total energies of the Pt-supported oxide film, of the adsorbate in the gas phase, and of the film with adsorbate, respectively.

The core-level binding energies have been computed in both initial and final state approximation. In initial state

calculations, after a full self-consistency with frozen core electrons is achieved, the Kohn–Sham equations are solved for core electrons inside the PAW sphere. In final state calculations, excitation of a single core electron is accounted by the corresponding core-excited ionic PAW potential. Due to the frozen core, this method accounts for screening by valence electrons but neglects screening by core ones. It provides an accurate estimate of relative core level binding energy shifts, but cannot yield absolute values for the core level binding energies [39]. In order to take FeO pristine film as reference, we have constructed models with FeO deposited on one side of the metal slab and with film of studied stoichiometry adsorbed on the other. We have verified that the results obtained have converged with respect to the size of vacuum and to Pt thickness (changes in core level binding energy shifts are less than 2 % when increasing the Pt thickness from 5 to 8 layers).

Vibrational frequencies have been computed within the harmonic approximation by using a central finite difference method (considering 0.02 Å displacements of the atoms in each Cartesian direction).

## 3 Results and Discussion

### 3.1 Gold Atom Adsorption

The ordered array of adatoms decorating the Moiré pattern and the low tendency to agglomerate highlighted by low-temperature STM measurements suggest a charged nature of Au atoms deposited on FeO/Pt(111) [29].

The calculations show that Au adatoms can adsorb on the film in two qualitatively different adsorption modes, characterized by opposite charge state [40, 41]. In the direct adsorption mode Au adsorbs on top of oxygen and is positively charged. In response to the positive charge of the adsorbate, the oxygen atom underneath relaxes towards the surface, increasing locally the film rumpling (by about 30 %). Conversely, in the flipped adsorption mode Au adsorbs on top of a Fe ion, which is pushed above the oxygen layer, Fig. 1. In this configuration the adatom is negatively charged and the local rumpling is reversed (by nearly −100 %). For both configurations, the structural distortion can be seen as an electrostatic response of the film to the adsorbate charging. Indeed, the dipole moment induced by the structural distortion opposes and partly compensates the one due to the adsorbate/substrate charge transfer [42].

The main signature of the charge state of the adatoms is related directly to the details of electronic structure. In Fig. 1 the Density of States (DOS) of the two configurations is reported. The Au electronic structure presents clear differences, in particular in the position of the Au 6*s* state, which can be measured by local spectroscopic probes, like Scanning Tunneling Spectroscopy (STS). In the direct configuration this state is above the Fermi level, while it is below the Fermi level in the flipped configuration, consistent with the two opposite charge states. Indeed, experimental STS spectra have helped the identification of the majority species observed after gold deposition at 5 K, since they present an Au-related feature at 500 mV above Fermi level, compatible with the direct adsorption mode [29, 40]. Also the preference for the Moiré region where the surface potential is the highest, Ref. [29], points to a positively charged adsorbate, as the charge transfer to the substrate is the most favorable in this region. In the calculations the flipped configuration is always preferred, but a recent study performed in the complete Moiré unit cell indicated the presence of a barrier of 0.4 eV to reach this state in the most populated Fe-fcc region [41], which could explain why it was not observed in the low-temperature STM experiments. On the other hand, the STS spectra of the minority Au atoms adsorbed in the other domains of the Moiré [29] (where the preferred flipped configuration can

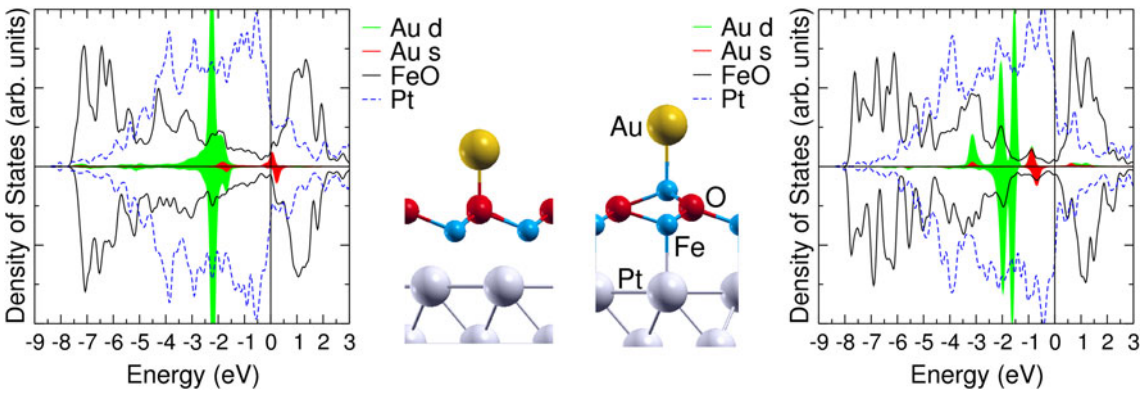


**Fig. 1** The two adsorption configurations for gold adatoms. *Left* Projected Density of States (PDOS) and structure of direct adsorption mode at Fe-fcc Moiré region. *Right* PDOS and structure of flipped adsorption mode at Fe-top Moiré region. *Gray*, *blue*, *red* and *yellow spheres* represent Pt, Fe, O and Au atoms, respectively

be reached without an energy barrier [41]) do not present Au-related features in the 0-1 V bias range, in agreement the computed DOS of the flipped configuration, Fig. 1. This is compatible with the simultaneous stabilization of both types of charged Au ad-atoms at different regions of the Moiré pattern, suggested in Ref. [41].

Besides the valence band spectroscopic features described above, other measurable signatures of the charge transfer can be traced. For instance the quenching of the Au magnetic moment clearly visible in the PDOS, Fig. 1, could be in principle monitored by EPR spectroscopy. However, no information could be traced on the sign of the charge transfer by this technique, which is additionally not suitable for this system because of the magnetic nature of the FeO substrate. A more promising tool is the use of CO as a probe molecule. STS data, in agreement with DFT PDOS, for CO dosed on pre-adsorbed Au has been already used as a further proof of the positively charged nature of Au adatoms adsorbed in Fe-fcc Moiré region, as CO adsorption causes the quenching of the 0.5 V signal [40]. Another observable which is very sensitive to the charge state of the metal particles is the CO vibrational frequency. No experimental data are available so far for this system, so that the calculations can provide a reference for further studies. We find that, on Au in direct adsorption mode at Fe-fcc Moiré site, CO forms a linear complex with a short Au–C distance (1.87 Å), as in the $Au^+CO$ gas phase complex. At variance with the latter, where the CO frequency is blue-shifted by 80 $cm^{-1}$ compared to free CO (computed frequency of free CO = 2136 $cm^{-1}$), for adsorbed $Au^+CO$ the vibrational frequency is red-shifted by about 20 $cm^{-1}$ due to the interaction with the substrate ($\nu$ = 2113 $cm^{-1}$). This is consistent with the computed elongation of the C–O bond (d(C–O) = 1.153 Å), compared to both the neutral and the positively charged gas-phase complexes (d(C–O) = 1.142 and 1.134 Å, respectively). In the flipped configuration an Au–CO tilted complex is stable, (d(Au–C) = 2.04 Å and $\alpha$(Au–C–O) = 149.2°), allowing an efficient overlap between filled Au 6*s* and empty CO $\pi^*$ orbitals. The resulting back-donation from Au to CO increases the C–O bond (d(C–O) = 1.154 Å) and causes a large red-shift of the CO stretching by almost 100 $cm^{-1}$ ($\nu$ = 2041 $cm^{-1}$).

### 3.2 $O_2$ Molecule Adsorption

The strong charge/structure coupling reported for Au also applies to molecular adsorbates, such as molecular oxygen. The interaction of oxygen with FeO/Pt(111) is particularly interesting as it has been reported that at high $O_2$ pressure the film incorporates oxygen, preferentially in the Fe-hcp region of the Moiré pattern [15, 16, 31]. Similarly to Au, two configurations exist for $O_2$ adsorbed on FeO/Pt(111), characterized by different charge states. In the first configuration the molecule is neutral, remains far from the surface and its interaction is negligible ($E_{ads} < 0.1$ eV), Fig. 2 (left panels); both the film and the molecule are hardly perturbed by their mutual interaction. On the contrary, in the second configuration the molecule interacts with a Fe ion, which flips above the oxygen plane, Fig. 2 (right panels). Here the molecule is in a superoxo state, as shown by the elongation of the O–O bond (1.353 Å compared to 1.236 Å of the neutral molecule) and by the spin doublet state, induced by the occupation of one of the spin-down components of $\pi^*$ $O_2$ orbital in the PDOS (Fig. 2, right panels). The different positions of the $O_2$-related states around the Fermi level can be monitored by STS, while infrared spectroscopy can detect the presence of the superoxo state (shifted by more then 450 $cm^{-1}$ with respect to the neutral molecule, either in the gas phase or adsorbed in the direct configuration) [43]. The charged configuration is only slightly more stable than the neutral one ($E_{ads}$ = 0.16 eV). We note that an even more stable charged state ($E_{ads}$ = 0.7 eV), with the molecule in peroxo state, was obtained at high oxygen coverage, associated to a flip of an entire Fe row [16].

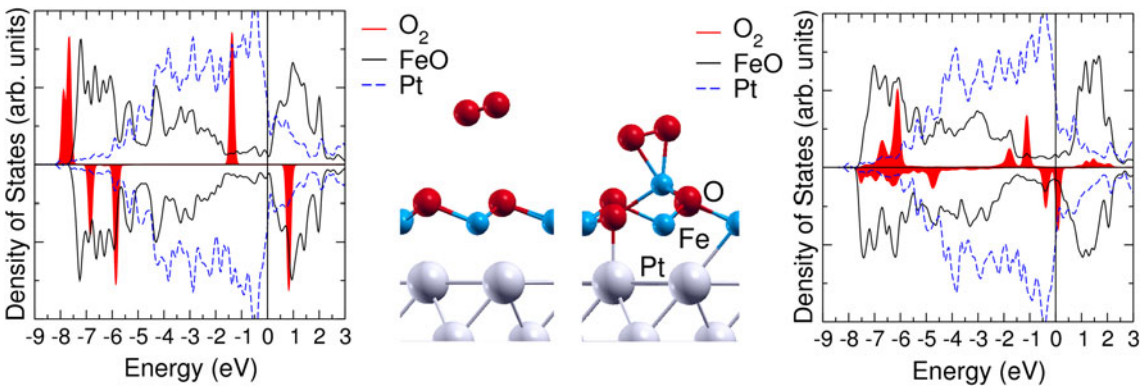


**Fig. 2** The two adsorption configurations for the oxygen molecule at the Fe-hcp Moiré region. *Left* PDOS and structure of neutral $O_2$. *Right* PDOS and structure of negatively charged $O_2$. *Gray*, *blue* and *red spheres* represent Pt, Fe and O atoms, respectively

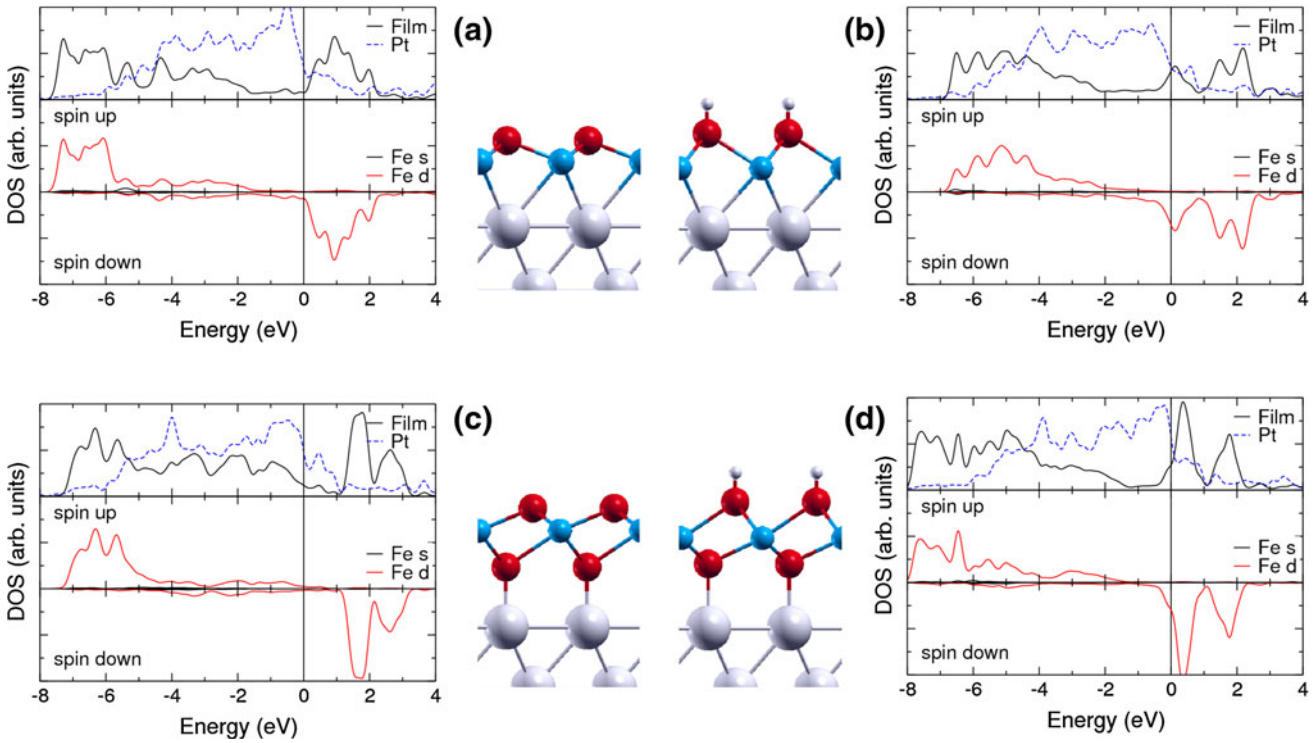


**Fig. 3** Structures and PDOS of dry and hydroxylated iron oxide films, stable on Pt(111) at different limits of the oxygen and water chemical potential: **a** FeO, **b** FeOH, **c** $FeO_2$, **d** FeOOH. *Gray*, *blue*, *red* and *white spheres* represent Pt, Fe, O and H atoms, respectively

### 3.3 Characterization of Dry and Hydroxylated Iron Oxide Monolayers

Oxygen charging represents an intermediate step for the formation of an oxygen-rich film, which drives the reactivity of this system towards CO [16]. Islands with $FeO_2$ stoichiometry are formed preferentially in Fe-hcp region, thus decorating the Moiré pattern [31].

A similar transformation, which maintains the long range order of the film and does not induce dewetting, has also been observed by exposing the FeO/Pt(111) film to air at room temperature [18]. The presence of hydroxyl groups suggests the formation of a FeOOH film. Spectroscopic measurements and ab initio phase diagrams for the sample exposed to a mixture of water and oxygen gases indicate that in water-poor conditions FeO transforms to $FeO_2$ at $\mu_O = -1.5$ eV (preferentially in the Fe-hcp region). In presence of water, the reduction of the films occurring in O-poor conditions is facilitated and results in the formation of an $FeOH_x$ ($x < 1$) film. At intermediate values of oxygen chemical potential, FeO with adsorbed molecular water is stable, while in oxygen-rich conditions a partly hydrated $FeOOH_x$ ($x < 1$) film is formed [18]. Although spectroscopic data and computed thermodynamics concur in identifying the different stable phases, a comparison between their measured and computed spectroscopic signatures is lacking. We will then compare the properties of the different phases, restricting our analysis to the Fe-hcp region where the $FeO_2$ is preferentially formed. For hydroxylated phases we consider the limit of full hydroxylation.

We have considered four structures obtained at different limits of oxygen and water chemical potential, Fig. 3 and Table 1. The valence band electronic structure visible in the PDOS panels in Fig. 3 shows that, due to the presence of the metal substrate, all oxide films have some metallic character. Moreover, the comparison of the Fe-projected DOS gives some information concerning iron oxidation state. In the case of $FeO_2$ iron is clearly in $d^5$ electronic configuration, signature of the $Fe^{+3}$ oxidation state. Conversely, Fe is formally $Fe^{+2}$ in FeO, although the PDOS shows some hybridization with Pt states, due to the proximity of the two metals at the interface. Upon hydrogenation the $d^6$ Fe electronic configuration is evident and is compatible with formal +2 oxidation state. For $FeO_2$, H adsorption causes a rigid downward shift of the oxide states, which for the full coverage considered here, pushes the Fe *d* minority states slightly below the Fermi level. In the experiments the hydrogenation is not complete, and the $Fe^{+3}$ oxidation state will likely be maintained. The different Fe oxidation states in O-poor and O-rich films agrees with the experimental XPS data in the Fe 2*p* regions, suggesting a transition from $Fe^{+2}$ to $Fe^{+3}$ upon transformation of FeO in FeOOH [18]. The behavior of Bader

**Table 1** Properties of dry and hydroxylated iron oxide films, stable on Pt(111) at different limits of the oxygen and water chemical potential: (a) FeO, (b) FeOH, (c) $FeO_2$, (d) FeOOH

| | Δz, Å[a] | q[b] | ΔΦ, eV | $CLS^{IS}$, eV[c] | $CLS^{FS}$, eV[c] | ν, $cm^{-1}$[d] |
|---|---|---|---|---|---|---|
| FeO | Pt–Fe: 2.134 | −0.26 | +0.31 | 0.0 | 0.0 | |
| | Fe–O: 0.702 | | | | | |
| FeOH | Pt–Fe: 1.991 | −0.37 | −3.63 | +0.6 | +2.3 | 3677 |
| | Fe–O: 1.157 | | | | | |
| | O–H: 0.974 | | | | | |
| $FeO_2$ | Pt–O: 1.981 | +0.30 | +1.72 | −0.6 (i); −1.4 (s) | −0.4 (i); −0.7 (s) | |
| | O–Fe: 1.208 | | | | | |
| | Fe–O: 0.750 | | | | | |
| FeOOH | Pt–O: 2.133 | +0.16 | −3.89 | +0.5 (i); +0.7 (s) | +0.9 (i); +2.5 (s) | 3769 |
| | O–Fe: 0.855 | | | | | |
| | Fe–O: 1.204 | | | | | |
| | O–H: 0.970 | | | | | |

[a] Inter-layer distances from the interface to the surface

[b] Interfacial charge transfer, estimated by the Bader charge of the Pt substrate, per oxide formula unit. $q > 0$ when electrons are transferred from Pt to the oxide

[c] O 1*s* core level binding energy shift (CLS) in initial (IS) and finale (FS) state approximation with respect to FeO/Pt(111), taken as reference. (i) = interface oxygen; (s) = surface oxygen

[d] Vibrational frequency for the symmetric OH stretching mode

charges on Fe ions is also consistent with Fe oxidation, although the absolute values are far from the formal charges.

The different film phases differ substantially by the sign and the nature of the interfacial charge transfer, Table 1. For bare FeO, due to the large electronegativity of Pt, electrons go from the oxide film to the metal substrate. This charge transfer is reinforced upon hydrogenation, as hydrogen forms surface hydroxyl groups and transfers its electron to the substrate. Conversely, in the $FeO_2$ case, the metal provides electrons to stabilize this unusual stoichiometry of the oxide film, with $Fe^{3+}$ and $O^{2-}$ formal oxidation states. In this case, since adsorbed hydrogen does also provide the required electrons, the charge transfer from Pt is reduced upon hydrogenation.

The film interlayer distances correlate with the charge transfers, in agreement with the electrostatic coupling of oxide monolayers on metal surfaces [22]. In the case of dry FeO and $FeO_2$ films, the surface rumpling is similar and is close to half of the bulk value for FeO in the (111) direction. On the other hand, for $FeO_2$ the O–Fe spacing on the interfacial termination of the film is almost twice as large. In both cases adsorption of hydrogen atoms increases the rumpling of the surface oxide layer.

We move now to another experimentally accessible quantity: the work function change with respect to Pt(111) surface, Table 1. We note an increase of the work function for FeO (induced principally by the large oxide rumpling at the considered Fe-hcp Moiré region) and $FeO_2$ (ascribable principally to the interfacial charge transfer). Conversely the presence of surface OH groups induces an extremely large work function decrease. The computed values are overestimated due to full OH coverage, which leads to a vertical configuration of all the OH groups. In the real system only a partial hydroxylation occurs and, since OHs are dynamical disoriented, their effective vertical dipole moment is smaller.

Experimental XPS data are available for FeO, FeOH and FeOOH [18]. The presence of hydroxyl groups gives rise to a O 1*s* XPS signal at higher binding energies with respect to the FeO main peak, shifted by 1.8 eV in absence of oxygen (attributed to FeOH species) and by 1.5 eV in presence of oxygen (FeOOH species) [18]. The core level shift to higher binding energy upon hydroxylation is confirmed by our calculations. While the magnitude of the shift is not well accounted in the initial state approximation, Table 1, the inclusion of final state effects gives results consistent with the experimental data. The crucial role of final state effects has also been reported for the calculation of O 1*s* CLS of OH groups on the MgO surface [44]. Concerning the $FeO_2$ film, for which no experimental data are available, we found a shift towards lower binding energies for both oxygen species, although the effect is more pronounced for the interfacial oxygen. In this case the shift is overestimated by the initial state approximation but reduced by final state effects, probably due to the screening of the metal substrate.

Also the OH stretching frequencies can help the identification of the FeOH and FeOOH species. In our calculations, this frequency for FeOOH is red-shifted by about

100 $cm^{-1}$ with respect to FeOH, Table 1. This agrees with the experimental IRAS data, attributing the structures in the range 3560–3590 $cm^{-1}$ to FeOH species, and the peak at 3650 $cm^{-1}$ to FeOOH ones [18]. We note that absolute values of computed frequencies are shifted by about 100 $cm^{-1}$ with respect to the experiments, partly because anharmonic effects are not included and partly due to limitations of our DFT-based ab initio approach.

## 4 Conclusions

The structural flexibility and the possibility to exchange electrons with the support are at the origin of alternative adsorption configurations on metal-supported ultra-thin films, which result in different charge states of adsorbates, and in opposite local polaronic distortions of the film. While clearly distinguishable by theoretical electronic band structure calculations, we have shown that these different configurations can be also identified experimentally by a variety of complementary spectroscopic signatures, ranging from valence and core levels spectroscopies, to vibrational frequencies of the ad-species.

In particular, the features of the calculated DOS and of experimental STS spectra in the vicinity of the Fermi level are very sensitive to the charge states of ad-species. This enables a precise assignment of adsorption configuration of different Au adatoms on FeO/Pt(111) observed in low temperature STM measurements. Similarly, core levels spectroscopy may be used to identify local transition from FeO to $FeO_2$ tri-layer structure upon exposure of the film to oxygen.

Moreover, in all cases the local features of the electronic structure are associated to detectable modifications of the vibrational characteristics. This concerns directly the stretching mode of $O_2$ ad-molecules adsorbed either neutrally or in superoxo state on FeO(111)/Pt(111), the stretching mode of CO molecules interacting with Au adatoms, either positively or negatively charged, and the stretching mode of hydroxyl groups formed at FeO/Pt or $FeO_2$/Pt oxide films.

We believe that the reported detailed theoretical mapping of the spectroscopic signatures for alternative adsorption configurations and adsorbate charge states provides a useful tool to identify the different species stabilized on the oxide ultra-thin film.

**Acknowledgments** We are grateful N. Nilius, S. Shaikhutdinov, M. Sterrer, and H.-J. Freund, for the long-lasting collaboration on the FeO/Pt(111) system. The authors thank the COST Action CM1104 "Reducible oxide chemistry, structure and functions" for support. Financial support from the Italian MIUR through the FIRB Project RBAP115AYN "Oxides at the nanoscale: multifunctionality and applications" (L.G. and G.P.) and the PRIN Project AKZSXY "Theory and first principle calculations of Auger spectra of magnetic systems" (L.G.) is gratefully acknowledged.

## References

1. Gates BC (1995) Chem Rev 95:511
2. Campbell CT (1997) Surf Sci Rep 27:1
3. Henry C (1998) Surf Sci Rep 31:235
4. Freund HJ (2002) Surf Sci 500:271
5. Santra AK, Goodman DW (2002) J Phys Cond Matt 14:R31
6. Cuenya BR (2010) Thin Solid Films 518:3127
7. Haruta H (2002) CATTECH 6:102
8. Yoon B, Häkkinen H, Landman U, Wörz AS, Antonietti JM, Abbet S, Judai K, Heiz U (2005) Science 307:403
9. Tauster SJ, Fung SC, Garten RL (1978) J Am Chem Soc 100:170
10. Connie MY, Yeung CMY, Yu KMK, Fu QJ, Thompsett D, Petch MI, Tsang SC (2005) J Am Chem Soc 127:18010
11. Nilius N (2009) Surf Sci Rep 64:595
12. Netzer FP, Allegretti F, Surnev S (2010) J Vac Sci Technol B 28:1
13. Giordano L, Pacchioni G (2011) Acc Chem Res 44:1244
14. Qin ZQ, Lewandowski M, Sun YN, Shaikhutdinov S, Freund HJ (2008) J Phys Chem C 112:10209
15. Sun YN, Qin ZH, Lewandowski M, Carrasco E, Sterrer M, Shaikhutdinov S, Freund HJ (2009) J Catal 266:359
16. Sun YN, Giordano L, Goniaksowski J, Lewandowski M, Qin ZH, Noguera C, Shaikhutdinov S, Pacchioni G, Freund HJ (2010) Angew Chem Int Ed 49:4418
17. Lewandowski M, Sun YN, Qin ZH, Shaikhutdinov S, Freund HJ (2011) Appl Catal A 391:407
18. Ringleb F, Fujimori Y, Wang HF, Ariga H, Carrasco E, Sterrer M, Freund HJ, Giordano L, Pacchioni G, Goniakowski J (2011) J Phys Chem C 115:19328
19. Weiss W, Ranke W (2002) Prog Surf Sci 70:1
20. Kim YJ, Westphal C, Ynzunza RX, Galloway HC, Salmeron M, Van Hove MA, Fadley CS (1997) Phys Rev B 55:13448
21. Ranke W, Ritter M, Weiss W (1999) Phys Rev B 60:1527
22. Goniakowski J, Noguera C (2009) Phys Rev B 79:155433
23. Giordano L, Cinquini F, Pacchioni G (2006) Phys Rev B 73:045414
24. Prada S, Martinez U, Pacchioni G (2008) Phys Rev B 78:235423
25. Rienks EDL, Nilius N, Rust HP, Freund HJ (2005) Phys Rev B 71:241404
26. Giordano L, Pacchioni G, Goniakowski J, Nilius N, Rienks EDL, Freund HJ (2007) Phys Rev B 76:075416
27. Zhang W, Li Z, Luo Y, Yang J (2009) J Phys Chem C 113:8302
28. Merte LR, Grabow LC, Peng G, Knudsen J, Zeuthen H, Kudernatsch W, Porsgaard S, Lægsgaard E, Mavrikakis M, Besenbacher F (2011) J Phys Chem C 115:2089
29. Nilius N, Rienks EDL, Rust HP, Freund HJ (2005) Phys Rev Lett 95:066101
30. Galloway HC, Sautet P, Salmeron M (1996) Phys Rev B 54:R11145
31. Giordano L, Lewandowski M, Groot IMN, Sun YN, Goniakowski J, Noguera C, Shaikhutdinov S, Pacchioni G, Freund HJ (2010) J Phys Chem C 114:21504
32. Dudarev SL, Botton GA, Savrasov SY, Humphreys CJ, Sutton AP (1998) Phys Rev B 57:1505
33. Perdew JP, Chevary JA, Vosko SH, Jackson KA, Pederson MR, Singh DJ, Fiolhais C (1992) Phys Rev B 46:6671
34. Blöchl PE (1994) Phys Rev B 50:17953
35. Bengone O, Alouani M, Blöchl PE, Hugel J (2000) Phys Rev B 62:16392

36. Kresse G, Hafner J (1993) Phys Rev B 47:R558
37. Kresse G, Furthmüller J (1996) Phys Rev B 54:11169
38. Bader RFW (1991) Chem Rev 91:983
39. Köhler L, Kresse G (2004) Phys Rev B 70:165405
40. Giordano L, Pacchioni G, Goniakowski J, Nilius N, Rienks EDL, Freund HJ (2008) Phys Rev Lett 101:026102
41. Ouyang R, Li WX (2011) Phys Rev B 84:165403
42. Goniakowski J, Noguera C, Giordano L, Pacchioni G (2009) Phys Rev B 80:125403
43. We found also a second charged superoxo state, less stable, where one single O atom interacts with the flipped Fe ion, with a Fe–O–O angle of 114°
44. Paz-Borboń LO, Hellman A, Grönbeck H (2012) J Phys Chem C 116:3545